フトオフ法により作製する.

PDMS 層は，上記とほぼ同様の手法により作製したものを鋳型とし，それを PDMS に転写することにより作製した.

B-1. 2. 酵素電極の作製法

本実験にて使用した酵素触媒は、辻村らにより報告されているものを用いた. *Aspergillus niger* 由来の Glucose oxidase (GOD) (EC 1.1.3.4) は和光純薬（株）より購入した. *Myrothecium sp.* 由来の Bilirubin oxidase (BOD) (EC 1.1.3.5) は天野エンザイム（株）より購入した. Poly(ethylene-glycol) diglycidyl ether (PEGDGE, Mn 520) は Aldrich より購入した. Poly(1-vinylpyridine) complexed with Os(4,4'-dimethyl-2,2' -bipyridine)$_2$Cl (PVI-Os) と Poly (4-vinylpyridine) complexed with Os(2,2'-bipyridine)$_2$Cl and quaternized with bromoethyl amine (PVP-Os) は第一化学薬品（株）より提供していただいたもの，もしくは文献に従い合成したものを用いた.

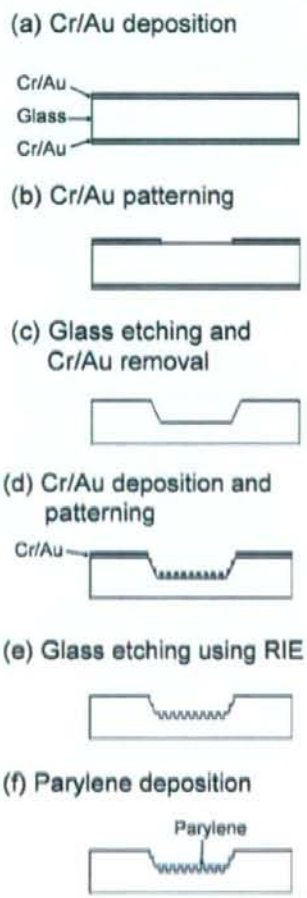

図 B-2 流路セルの作製手順

アノードの酵素膜修飾は，5 μL の PVI-Os 溶液 (25 mg mL^{-1})，2 μL の GOD 溶液 (20 mg mL^{-1}) および 1.2 μL の PEGDGE 溶液 (2.5 mg mL^{-1}) を混合し，その 0.5 μL を金電極 (1 mm 直径) に塗布し，室温で一晩ほど乾燥させることにより行った．同様にカソードでは，5 μL の PVP-Os 溶液 (25 mg mL^{-1})，2 μL の BOD 溶液 (20 mg mL^{-1}) および 1.2 μL の PEGDGE 溶液 (2.5 mg mL^{-1}) を混合し，その 0.5 μL を金電極 (直径 1 mm) に塗布することにより行った．酵素膜の乾燥過程において，PEGDGE が両端に有すエポキシ基が，水溶性のポリマーや酵素の有すアミノ基，もしくはイミダゾール基同士と反応し架橋構造を作ることにより，水に不溶なハイドロゲル状の酵素触媒薄膜を形成する．また，このようにして作製した酵素膜は燃料極，酸素極において，それぞれ以下のような反応を触媒する.

燃料極: glucose → gluconolactone + $2H^+ + 2e^-$

酸素極: $O_2 + 4H^+ + 4e^- \rightarrow 2H_2O$

GOD にてグルコースを酸化することで得られた電子は，電子メディエータであるオスミウム錯体を介して電極へ受け渡され，外部回路を通過した後，酸素極にてオスミウム錯体，BOD を介し酸素へと受け渡される．このようにして，本研究ではグルコース / 酸素型のバイオ燃料電池とした.

B-1. 3. 測定法

試料表面の撥水性は，1 μL の蒸留水の液滴を用いた接触角測定により評価した．その際の結果は，各条件で作製した材料上の異なる三点で測定したものの平均をプロットしている．

電気化学測定は，室温で，0.1 M NaCl と 0.1 M グルコースを含む 50 mM リン酸緩衝液 (pH 7.0) を用いて行った．またその際には電気化学測定システム (Model 600S, BAS) を用いた．マイクロ流路中への定常的な送液はマイクロシリンジポンプ (Kd Scientific, Model 210) を用いて行った．

C. 研究結果と D. 考察

C-1. 超撥水表面の作製

図 C-1(a), (b) には，パターニングした Cr/Au をマスクとして RIE を施したガラス基板の走査型電子顕微鏡 (scanning electron microscope (SEM)) 画像を示す．これらの画像より，微細突起アレイ (高さ 20 μm, 直径 15 μm, 間隔 15 μm) を作製できたことが見て取れる．この微細突起の側面は傾斜がかっているが，これは RIE の際に Cr/Au マスクの端部におけるイオンの反射によるもの，もしくはそれとマスク自体のエッチングによるものと考えられる．また，図 C-1(c),(d)には顕微鏡写真を示す．それぞれ PDMS，ガラス基板上に作製したマイクロ流路のバルブ部に，微細突起アレイをパターニングできていることが確認できた．

ここで，表面の撥水性は，材料表面滴下した 1 μL の液滴の見た目の接触角 (θ_c) を測定することにより評価した．図 C-2 (a)-(c) は，(a) ガラス基板上, (b) parylene を蒸着した平らなガラス基板上，及び (c) parylene を蒸着した微細突起アレイ上における液滴の写真を示している．これらは，θ_c が 150° を超える超撥水表面を作製するためには，材料自体の疎水

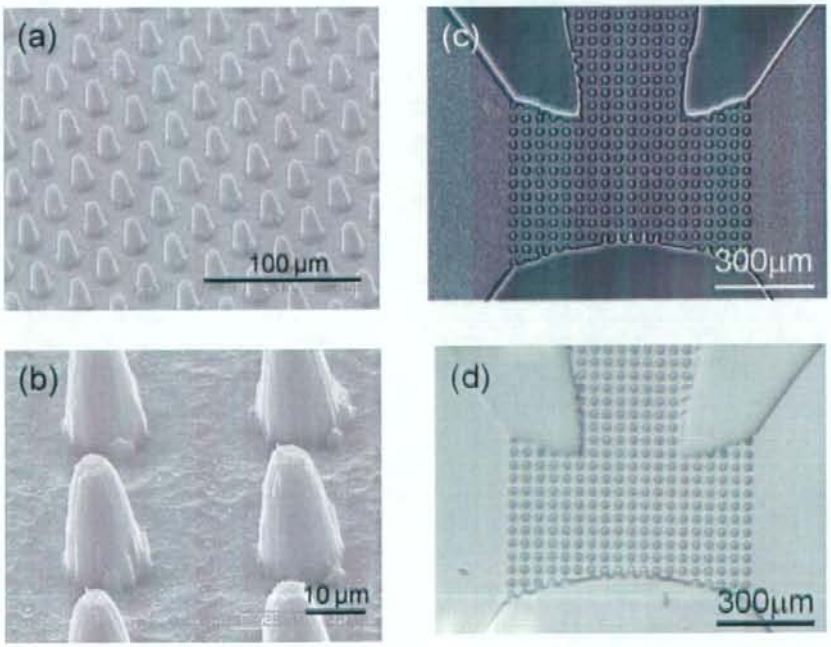

図 C-1　作製した基板の(a)(b)SEM 画像と(c)(d)顕微鏡画像

性に加え，微細な表面構造が重要であることを示している．また図 C-2 (d) に示すように，微細突起を作製することで，PDMS 上でも高い撥水性が得られることがわかった．図 C-2 (e) と (f) には微細突起の直径と間隔を変化させた際の θ_c を示しており，そこでは直径 15 μm の微細突起が 15 μm 間隔で配列しているものが最も高い θ_c が得られた．

ここで，化学的に疎水性で荒い表面においては，液一個体一空気の三相界面が現れ，構造体の谷部に空気の層を形成すると考えられている．空気の θ_c が 180°であるため，この空気の層の撥水性への寄与は大きいものである．このような条件下において見た目の接触角 θ_c を見積もるためには，通常以下の変形された Cassie-Baxter 式 (式(1)) が適用される．

$$\cos\theta_c = f(1+\cos\theta)-1 \qquad (1)$$

ここで，f は個体分率，θ は材料本来（平滑な表面）の接触角である．式 (1) は f が小さいほど（間隔が広い，小さい突起），材料と液滴との接触面積を減らし，空気と液滴の接触面積を増やすことができるため，大きな θ_c が得られることを示している．しかしながら実際のところ，f が小さすぎる条件では，突起間への液滴の侵入を防ぐことができないため，結果として θ_c が小さくなってしまう．これらの議論により，図 C-1 (e) と(f)で接触角の最適値が現れたことを説明できる．つまり，最適値よりも f の小さな領域においては，液一材料間の接触面積が液滴の量に対して小さくなりすぎた結果，液滴が突起間に侵入してきているものと考えられる．また，円錐状の突起形状（図 C-1）もこのような溶液の侵入を容易にしてしまっているものと考えられる．

PDMS で作製した微細突起アレイの θ_c についても，図 C-2 (e) と(f) に示すような実験を行い評価したところ，ガラス基板上での結果と同様，直径 15 μm，間隔 15 μm のときに最適値を示し，その時の θ_c はおよそ 170 °

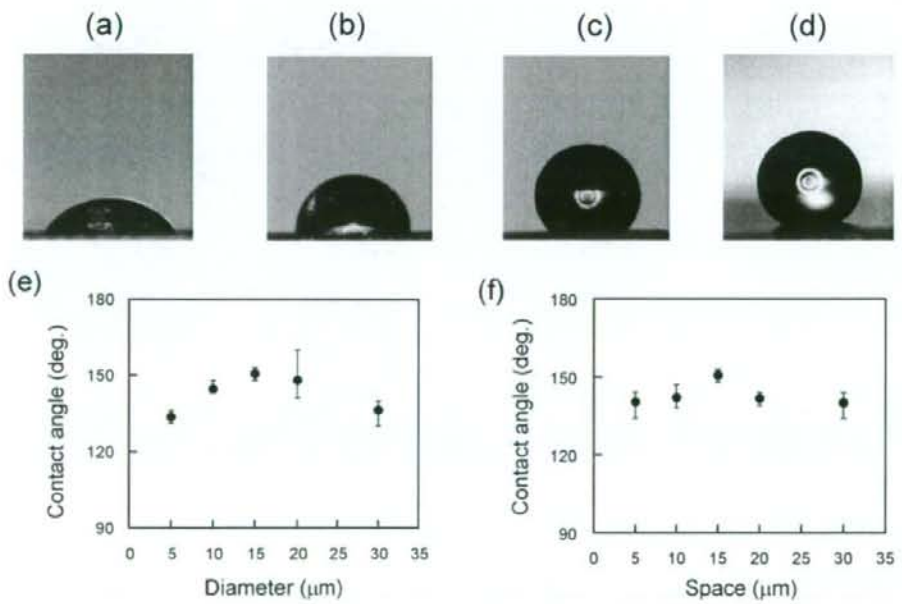

図 C-2 (a)ガラス基板，(b)Parylene 被膜ガラス基板，(c)突起構造を作製した Parylene 被膜ガラス基板，(d)突起構造を作製した PDMS 上の液滴の写真．(e)突起径と(f)突起間隔を変えた基板上で得られた液滴の接触角．

と非常に大きなものが得られた．PDMS と parylene の平滑な表面上における θ が 100 ° 程度と同程度であるにも関わらず，PDMS で作製した微細突起アレイの接触角が高くなった原因については明らかではないが，おそらく化学的，構造的な性質に加え，PDMS の機械的な性質といったものが関係しているのではないかと推測している．ここで，0.1 M のグルコースを含む緩衝液を用いた場合においても，蒸留水を用いた場合と同様の接触角を得ることができた．

C-1. 2. 空気バルブの評価とバイオ燃料電池の直列化

図 B-1 に示すように，作製したガラス製のマイクロ流路と PDMS 製のマイクロ流路を張り合わせ，ポリエチレン製のチューブをインレットとアウトレットに金属製のコネクタを介して接続し，流路デバイスの性能評価を行った．Fig. 4.7 は深さ 40 μm のマイクロ流路セル間に配置した超撥水領域の溶液注入中の顕微鏡写真である．ここで，溶液が流れている際にも超撥水領域が完全に溶液が満たされてしまっていないことに注目したい（図 C-3(b)）．このような状態というのは，図 C-3(b) の下図に示したようにセル間の超撥水領域を，溶液が小さな液滴状もしくは霧状で通過している状態であると考えられ，その際，それぞれのセルのイオン電導は絶縁されていることが予想される．ここで，送液を止めることにより空気リザーバから超撥水領域に空気が導入され，それぞれのセルはよりはっきりと分断された（図 C-3(c)）．なお，この空気バルブは 1 ～ 10 μL min^{-1} で安定した動作を示した．より高い流速下においては溶液の空気リザーバ部への侵入が問題となった．流路高さの影響についても評価したところ，流路高さの低い条件下（～ 40 μm）において良好な動作を示した．これは体積当たりの表面積比が増加することで，溶液に対して，より表面の撥水性の影響を顕著に与えられたためと考えられる．

最後に，この空気バルブシステムを利用したバイオ燃料電池の自動直列化について検討した．図 B-1 に示すように，グルコース/O_2 型バイオ燃料電池は三対の酵素修飾アノード，カソードからなっている．5 μL min^{-1} の流速下において 1 対のバイオ燃料電池から得られる開回路電圧（open circuit voltage (OCV)）は約 0.35 V，最大出力電流密度は約 0.2 mA cm^{-2}，最大出力電力密度は約 0.02 mW cm^{-2} で

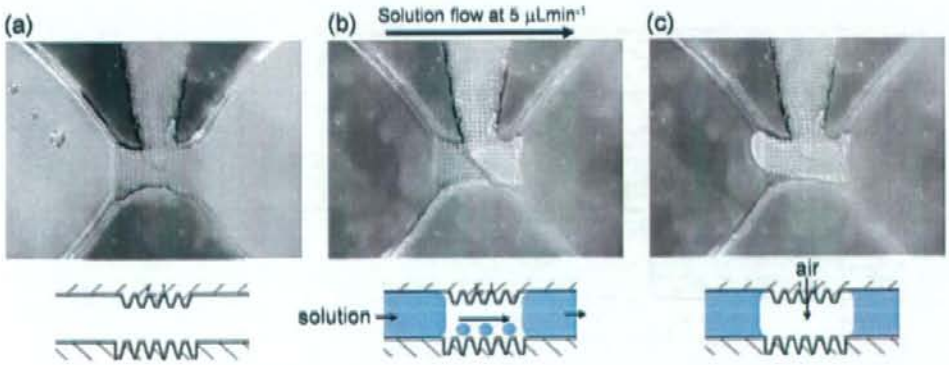

図 C-3　セル間のバルブ部の顕微鏡写真．(a)溶液注入前，(b)溶液注入中，(c)送液停止後．

あった．最大電流密度は報告されている値よりも小さいものであったが，これは本研究で用いた燃料溶液中の酸素濃度（空気飽和溶液）が文献で用いられていたもの（酸素飽和溶液）よりも低かったためである．ここで，直列型バイオ燃料電池のコンセプトを証明するため，燃料の注入，再注入操作に伴う開回路電圧値の推移を測定した．図 C-4(a)はその際得られた典型的な OCV の一例である．時間 0 において，0.1 M グルコースを含む電解溶液をマイクロ流路中に 5 μL min^{-1} の流速で注入し，数分で溶液は全セルに満たされた．ここで，送液中における OCV は 0.65 V ほどであり，おおよそ 2 つのバイオ燃料電池が直列化された電圧であった．この現象は 2 つの空気バルブのうち 1 つのみが閉じている（溶液が分断）していることを示唆している．空気バルブの写真(図 C-3(b)) から推測されることとしては，

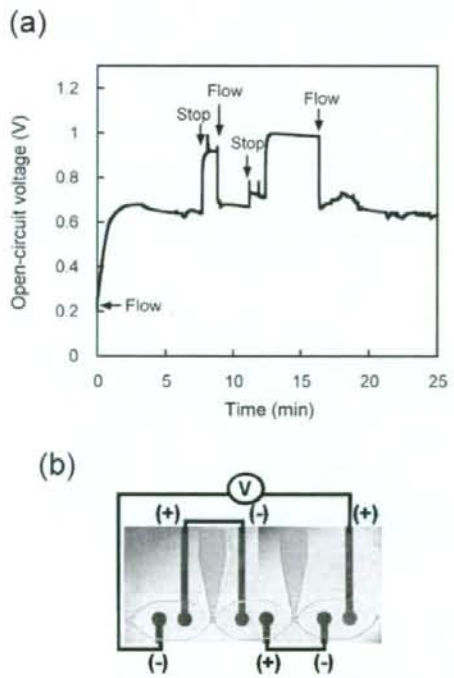

図 C-4 (a)直列化バイオ燃料電池の出力電圧．(b) 直列化バイオ燃料電池の顕微鏡写真と電気配線．

燃料溶液は微小な液滴や霧として“閉じた”空気バルブを通過しているのではないかということである．ここで，送液を停止することで，OCV は速やかに 1 V 程度に上昇した．これは 2 つのバルブともに機能し，3 つのバイオ燃料電池が完全に直列化していることを示している．また図 C-4 に示されるように，このバイオ燃料電池から出力される OCV は，送液操作により可逆的に応答することもわかった．高い撥水性を有すフッ化炭素樹脂などの材料の利用や，流体現象に配慮した流路設計によって，より安定したセルの直列化が可能になると考えられる．

E. 結論

本章では，RIE 等の微細加工により作製した微細突起アレイ（高さ 20 μm，直径 15 μm，間隔 15 μm）からなる超撥水領域（θ_c > 150°）を空気バルブとして利用したバイオ燃料電池の直列化システムを実証し，1 V 以上の開回路電圧を得ることができた．この超撥水領域はほぼ自動で作動する空気バルブとして可逆的に機能し，バイオ燃料電池セル間のイオン絶縁を実現することで，それに伴う OCV の変化を観測することができた．材料やセル構造の最適化によるバルブの安定駆動により，生体内でも利用可能な直列型バイオ燃料電池となることが期待できる．また、本研究では，PDMS とガラス基板からなるデバイスを作製したが，同様の作製手法により，すべてをプラスチックで構成することができるため，フレキシブルで容易に使い捨て可能なエネルギーデバイスとすることもできる．

F. 健康危険情報

なし

G. 研究発表

G-1. 論文

1. Miniature Biofuel Cells toward

Medical Applications. Togo M, Yatagawa Y, Oike M, Kaji H, Abe T, Nishizawa M. Technical Digest PowerMEMS 2008: 65-68, 2008.

2. Miniatured Biofuel Cells Automatically Relayed for Longer-term Power Generation. Oike M, Togo M, Kaji H, Abe T, Nishizawa M. Technical Digest PowerMEMS 2008: 441-444, 2008.
3. バイオ燃料電池マイクロシステムと体液発電への取り組み
西澤松彦
Electrochemistry 76: 916-919, 2008.

G-2. 学会発表

1. 微細加工技術を用いた小型バイオ燃料電池の開発
都甲 真, 森本恵司, 大池真人, 浅井達也, 梶 弘和, 安部 隆, 西澤松彦
電気化学会第 75 回大会 (2008.3.29-31)
2. Development of High Performance Microfluidic Biofuel Cell. Togo M, Asai T, Oike M, Kaji H, Abe T, Nishizawa M. Biosensors 2008 (2008.5.14-16)
3. Structural studies on microfluidic biofuel cells. Nishizawa M, Togo M, Morimoto K, Kaji H, Abe T. 213th ECS Meeting (2008.5.18-22)
4. Stepwise Electric Power Generation for Prolonging Lifetime of Miniaturized Biofuel Cell. Togo M, Oike M, Kaji H, Abe T, Nishizawa M. PRiME 2008 (2008.10.12-17)
5. Miniature Biofuel Cells toward Medical Applications. Togo M, Yatagawa Y, Oike M, Kaji H, Abe T, Nishizawa M. PowerMEMS 2008 (2008.11.9-12)
6. Miniatured Biofuel Cells Automatically Relayed for Longer-term Power Generation. Oike M, Togo M, Kaji H, Abe T, Nishizawa M. PowerMEMS 2008 (2008.11.9-12)
7. バイオ燃料電池における時差式発電システムの検討
大池真人, 都甲 真, 梶 弘和, 安部 隆, 西澤松彦
第 18 回化学とマイクロ・ナノシステム研究会 (2008.12.7-9)

G-3.新聞報道

なし

H.知的所有権の取得状況

なし

研究成果の刊行に関する一覧表

書籍

著者名	論文タイトル	書籍全体の編集者名	書籍名	出版社名	出版地	出版年	ページ
Matsuhiko Nishizawa	MINIATURIZED MICROFLUIDIC BIOFUEL CELLS	Takami Yamaguchi	Nano-Biomedical Engineering 2009 : A Tohoku University Global COE Programme Proceedings	Imperial College Press	London	2009	235-244

雑誌

発表者氏名	論文タイトル名	発表誌名	巻号	ページ	出版年
Kamiya A, Kawada T, Yamamoto K, Mizuno M, Shimizu S, Sugimachi M.	Upright tilt resets dynamic transfer function of baroreflex neural arc to minify the pressure disturbance in total baroreflex control.	J Physiol Sci	58	189-198	2008
Kawada T, Yamazaki T, Akiyama T, Kitagawa H, Shimizu S, Mizuno M, Li M, Sugimachi M.	Vagal stimulation suppresses ischemia-induced myocardial interstitial myoglobin release.	Life Sci	83	490-495	2008
Miyamoto T, Kawada T, Yanagiya Y, Akiyama T, Kamiya A, Mizuno M, Takaki H, Sunagawa K, Sugimachi M.	Contrasting effects of presynaptic alpha2-adrenergic autoinhibition and pharmacologic augmentation of presynaptic inhibition on sympathetic heart rate control.	Am J Physiol Heart Circ Physiol	295	H1855-1866	2008
Mizuno M, Kamiya A, Kawada T, Miyamoto T, Shimizu S, Shishido T, Sugimachi M.	Accentuated Antagonism in Vagal Heart Rate Control Mediated through Muscarinic Potassium Channels.	J Physiol Sci	58	381-388	2008
Sugimachi M, Kawada T, Yamamoto H, Kamiya A, Miyamoto T, Sunagawa K.	Modification of autonomic balance by electrical acupuncture does not affect baroreflex dynamic characteristics.	Conf Proc IEEE Eng Med Biol Soc	1	1981-1984	2008
Yamamoto K, Kawada T, Kamiya A, Takaki H, Shishido T, Sunagawa K, Sugimachi M.	Muscle mechanoreflex augments arterial baroreflex-mediated dynamic sympathetic response to carotid sinus pressure.	Am J Physiol Heart Circ Physiol	295	H1081-H1089	2008

Yamamoto H, Kawada T, Kamiya A, Kita T, Sugimachi M.	Electroacupuncture changes the relationship between cardiac and renal sympathetic nerve activities in anesthetized cats.	Auton Neurosci	144	43-49	2008
Uemura K, Sunagawa K, Sugimachi M.	Computationally managed bradycardia improved cardiac energetics while restoring normal hemodynamics in heart failure.	Ann Biomed Eng	37	82-93	2009
Kashihara K, Kawada T, Sugimachi M, Sunagawa K.	Wavelet-based system identification of short-term dynamic characteristics of arterial baroreflex.	Ann Biomed Eng	37	112-128	2009
Makoto Kawasaki, Ryuji Kohno	Position Estimation Method of Medical Implanted Devices Using Estimation of Propagation Velocity inside Human Body	IEICE TRANS. Special Section on Medical Information and Communications Technologies	Vol. E92-B, No.02	pp.403-409	2009
Makoto Kawasaki, Ryuji Kohno	A TOA based Positioning Technique of Medical Implanted Devices	The Third International Symposium on Medical Information and Communication Technology(ISMICT2009)			2009
Shun Nagamine, Ryuji Kohno	Design of Communication Model Suitable for Implanted Body Area Networks	The Third International Symposium on Medical Information and Communication Technology(ISMICT2009)			2009
Hideki Mochizuki, Makoto Kawasaki, Shun Nagamine, Igor Dotlic, Ryuji Kohno	Performance Analysis of Pulsed Chirp UWB Schemes used Hopping Sequence for Wearable Wireless Body Area Network	The Third International Symposium on Medical Information and Communication Technology(ISMICT2009)			2009
Koji Enda, Ryuji Kohno	Routing Algorithm to Decrease Transmission Delay and Traffic Quantity using Priority Area in Sensor	The Third International Symposium on Medical			2009

	Network of Hospital	Information and Communication Technology(ISMICT2009)			
望月 英希,河嵜 誠,長嶺 駿,田井 和成, 原田 浩樹,河野 隆二	ウェアラブルボディエリアネットワークに適したUWB通信方式の研究	電子情報通信学会 第1回MICT研究会		pp.105-113	2008
河嵜誠、長嶺駿、河野隆二	伝搬速度推定による医療用埋め込み機器の位置推定法に関する検討	第31回情報理論とその応用シンポジウム(SITA0208)	2.5.3	pp.959-964	2008
長嶺 駿, 河嵜 誠, 河野 隆二	生体内センサネットワークにおける消費電力と熱影響を考慮した通信モデルの設計	第31回情報理論とその応用シンポジウム(SITA0208)	9.1.5	pp. 959-964	2008
望月 英希,河嵜 誠,長嶺 駿,河野 隆二	Wearable Wireless Body Area Network環境下におけるホッピング系列を用いたPulsed Chirp UWB方式の特性評価	第31回情報理論とその応用シンポジウム(SITA2008)	3.3.1	pp.287-292	2008
望月 英希,河嵜 誠,長嶺 駿,河野 隆二	Wearable Wireless Body Area Network環境下におけるピコネット間干渉を考慮した通信特性の評価	電子情報通信学会 2008年ソサイエティ大会	A-5-20	pp.107	2008
Togo M, Yatagawa Y, Oike M, Kaji H, Abe T, Nishizawa M	Miniature Biofuel Cells toward Medical Applications	Proceedings of PowerMEMS		65-68	2008
Oike M, Togo M, Kaji H, Abe T, Nishizawa M	Miniatured Biofuel Cells Automatically Relayed for Longer-term Power Generation	Proceedings of PowerMEMS		441-444	2008
西澤松彦	バイオ燃料電池マイクロシステムと体液発電への取り組み	Electrochemistry	76	916-919	2008

REGULAR PAPER

J. Physiol. Sci. Vol. 58, No. 3; Jun. 2008; pp. 189–198
Online May 13, 2008; doi:10.2170/physiolsci.RP004308

Upright Tilt Resets Dynamic Transfer Function of Baroreflex Neural Arc to Minify the Pressure Disturbance in Total Baroreflex Control

Atsunori KAMIYA[1], Toru KAWADA[1], Kenta YAMAMOTO[2], Masaki MIZUNO[1], Shuji SHIMIZU[1], and Masaru SUGIMACHI[1]

[1]Department of Cardiovascular Dynamics, National Cardiovascular Centre Research Institute, Osaka, Japan; and [2]Consolidated Research Institute for Advanced Science and Medical Care, Waseda University, Tokyo ,162-0041 Japan

Abstract: Maintenance of arterial pressure (AP) under orthostatic stress against gravitational fluid shift and pressure disturbance is of great importance. One of the mechanisms is that upright tilt resets steady-state baroreflex control to a higher sympathetic nerve activity (SNA). However, the dynamic feedback characteristics of the baroreflex system, a hallmark of fast-acting neural control, remain to be elucidated. In the present study, we tested the hypothesis that upright tilt resets the dynamic transfer function of the baroreflex neural arc to minify the pressure disturbance in total baroreflex control. Renal SNA and AP were recorded in ten anesthetized, vagotomized and aortic-denervated rabbits. Under baroreflex open-loop condition, isolated intracarotid sinus pressure (CSP) was changed according to a binary white noise sequence at operating pressure ± 20 mmHg, while the animal was placed supine and at 60° upright tilt. Regardless of the postures, the baroreflex neural (CSP to SNA) and peripheral (SNA to AP) arcs showed dynamic high-pass and low-pass characteristics, respectively. Upright tilt increased the transfer gain of the neural arc (resetting), decreased that of the peripheral arc, and consequently maintained the transfer characteristics of total baroreflex feedback system. A simulation study suggests that postural resetting of the neural arc would significantly increase the transfer gain of the total arc in upright position, and that in closed-loop baroreflex the resetting increases the stability of AP against pressure disturbance under orthostatic stress. In conclusion, upright tilt resets the dynamic transfer function of the baroreflex neural arc to minify the pressure disturbance in total baroreflex control.

Key words: baroreflex, blood pressure, sympathetic nervous system.

Since human beings are often under orthostatic stress, the maintenance of arterial pressure (AP) under orthostatic stress against gravitational fluid shift is of great importance. During standing, a gravitational fluid shift directed toward the lower part of the body would cause severe postural hypotension if not counteracted by compensatory mechanisms [1]. Arterial baroreflex has been considered to be the major compensatory mechanism [1–3], since denervation of baroreceptor afferents causes profound postural hypotension [4].

The baroreflex system consists of two subsystems: the neural arc that represents the input-output relationship between baroreceptor pressure and sympathetic nerve activity (SNA), and the peripheral arc that represents the relationship between SNA and systemic AP. Recently, we investigated the steady-state functional structure of these systems under orthostatic stress [5], and reported that upright tilt shifted the baroreflex peripheral arc to a lower AP for a given SNA. However, upright tilt reset the baroreflex neural arc to a higher steady state SNA. The resetting compensated for the blunted responsiveness of the peripheral arc and contributed to prevent postural hypotension [5].

In addition to the steady state characteristics [6, 7], the dynamic characteristics are other hallmark of the baroreflex system. It is because the system is a fast-acting neural control that quickly negative-feedback controls and stabilises AP against pressure disturbance in contrast to the slow-acting hormonal and humoral systems [8]. Earlier studies reported that the dynamic characteristics in supine position have a high-pass (fast) neural arc that may compensate for the low-pass (slow) peripheral arc to achieve rapid and stable AP regulation [8]. The importance of the dynamic characteristics in AP control increases under orthostatic stress that can cause postural hypotension. However, little is known about the dynamic characteristics of the baroreflex system in upright posture.

Because the gravitational body fluid shift decreases the effective circulatory blood volume [1, 9], we speculated that upright tilt may attenuate the dynamic transfer function from SNA to AP in the baroreflex peripheral arc.

Received on Mar 18, 2008; accepted on May 9, 2008; released online on May 13, 2008; doi:10.2170/physiolsci.RP004308
Correspondence should be addressed to: Atsunori Kamiya, Department of Cardiovascular Dynamics, National Cardiovascular Centre Research Institute, Osaka, 565-8565 Japan. Tel: +81-6-6833-5012, Fax: +81-6-6835-5403, E-mail: kamiya@ri.ncvc.go.jp

Moreover, if the upright tilt resets the dynamic characteristics of the neural arc in addition to resetting the steady state SNA reported previously [5], it would compensate for a blunted pressor response of the baroreflex peripheral arc and contribute to maintain the stability and quickness of the total baroreflex system. Accordingly, we hypothesized that upright tilt resets dynamic transfer function of baroreflex neural arc to minify the pressure disturbance in total baroreflex control.

In the present study, we identified the transfer functions of two baroreflex subsystems (the neural and peripheral arcs) separately in 60° upright posture, while opening the baroreflex negative feedback loop by vascular isolation of carotid sinus regions [8]. In addition, by connecting the subsystem transfer functions in series and closing them, we investigated the dynamic transfer characteristics and the stability against pressure disturbance of total baroreflex arc system in upright posture.

MATERIAL AND METHODS

Animals were cared for in strict accordance with the Guiding Principles for the Care and Use of Animals in the Field of Physiological Science approved by the Physiological Society of Japan. Ten Japanese white rabbits weighing 2.4–3.3 kg were initially anesthetized by intravenous injection (2 ml/kg) of a mixture of urethane (250 mg/ml) and α-chloralose (40 mg/ml). Anesthesia was maintained by continuously infusing the anaesthetics at a rate of 0.33 ml/kg/h using a syringe pump (CFV-3200, Nihon Kohden, Tokyo). The rabbits were mechanically ventilated with oxygen-enriched room air. Bilateral carotid sinuses were isolated vascularly from systemic circulation by ligating the internal and external carotid arteries and other small branches originating from the carotid sinus regions. The isolated carotid sinuses were filled with warmed physiological saline pre-equilibrated with atmospheric air, through catheters inserted via the common carotid arteries. Intra-carotid sinus pressure (CSP) was controlled by a servo-controlled piston pump (model ET-126A, Labworks; Costa Mesa, CA). Bilateral vagal and aortic depressor nerves were sectioned in the middle of the neck region to eliminate reflexes from the cardiopulmonary region and the aortic arch. Systemic AP was measured using a high-fidelity pressure transducer (Millar Instruments; Houston, TX) inserted retrograde from the right common carotid artery below the isolated carotid sinus region. Body temperature was maintained at around 38°C with a heating pad.

The left renal sympathetic nerve was exposed retroperitoneally. A pair of stainless steel wire electrodes (Bioflex wire AS633, Cooner Wire) was attached to the nerve to record renal SNA. The nerve fibers peripheral to electrodes were ligated securely and crushed to eliminate afferent signals. The nerve and electrodes were covered with a mixture of silicone gel (Silicon Low Viscosity, KWIK-SIL, World Precision Instrument, Inc., FL) to insulate and immobilize the electrodes. The preamplified SNA signal was band-pass filtered at 150–1,000 Hz. The nerve signal was full-wave rectified and low-pass filtered with a cutoff frequency of 30 Hz to quantify the nerve activity.

Protocols. Both protocols 1 and 2 were performed on each of eight animals. After the surgical preparation, the animal was maintained supine (0°) on a tilt bed. To stabilize the posture, the head was fixed full-frontal to the bed by strings, and the body and legs were rigged up in a clothes-like bag. Before performing protocols 1 and 2, we confirmed that the nerve activity measured in supine position was SNA. CSP was decreased stepwise from 100 mmHg to 40 mmHg in decrements of 20 mmHg, and then increased stepwise to 100 mmHg in increments of 20 mmHg. Each pressure step was maintained for 60 s. In all animals, a decrease in CSP increased SNA, whereas an increase in CSP decreased SNA (Fig. 1), indicating that the nerve activity recorded was SNA.

Protocol 1: The animal was placed supine. CSP was firstly matched with systemic AP to obtain the operating AP under the baroreflex closed-loop condition. After at least 5 minutes of stabilization, the SNA and AP were recorded for 10 min to obtain closed-loop baseline values. The data were stored on the hard disk of a dedicated laboratory computer system for analysis at a sampling rate of 200 Hz using a 12-bit analog-to-digital converter. The averaged AP over 10 min was defined as the operating AP in

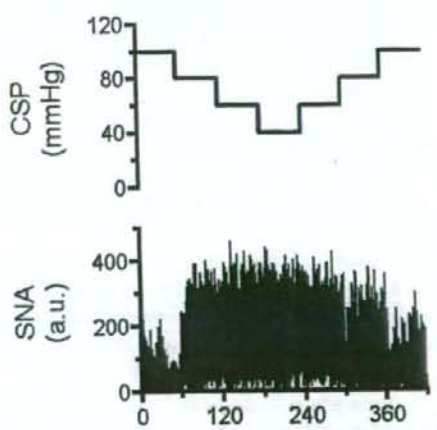

Fig. 1. Representative data of one rabbit in supine position, showing time series of carotid sinus pressure (CSP) and sympathetic nerve activity (SNA). CSP was decreased stepwise from 100 mmHg to 40 mmHg in decrements of 20 mmHg, and then increased stepwise to 100 mmHg in increments of 20 mmHg. Each pressure step was maintained for 60 s. A decrease in CSP increased SNA, whereas an increase in CSP decreased SNA, indicating that the nerve activity recorded was SNA. a.u., arbitrary unit.

supine position. Then, after at least 5 min of stabilization, CSP was randomly changed by 20 mmHg above or below the operating AP every 500 ms according to a binary white noise sequence for which the input power spectrum of CSP was reasonably flat up to 1 Hz [10]. The variables were recorded for a 10-min period and stored.

Protocol 2: CSP was firstly matched with systemic AP via a servo-controlled piston pump to obtain the actual operating pressure under baroreflex closed-loop conditions in supine and 60° upright postures. The animal was maintained supine for 10 min, and then tilted upright to 60° within 10 s by inclining the tilt bed to 60° and dropping the lower regions of the rabbit with the fulcrum set at the level of the carotid sinus. The 60° upright posture was maintained for 10 min for stabilization. Since the clothes-like bag stabilized the posture of the animal, there was no additional mechanical movement that reduced the quality of measurements. The position of the head remained almost fixed during the tilt to minimize vestibular stimulation. Thereafter, the average AP over the next 10 min was defined as the operating AP in upright tilt position. Then, after at least 5 min of stabilization, CSP was randomly changed according to a white noise sequence for 10 min as in protocol 1.

Data analysis. SNA signals were normalized by the following steps. First, the post-mortem noise level was assigned 0 arbitrary unit (a.u.). Second, SNA signals during the 10-min closed-loop baseline recording in protocol 1 (supine position) were averaged over 1 min, and assigned 100 a.u. Finally, the other SNA signals in all protocols were normalized to these values.

In both protocols 1 and 2, the transfer functions (gain and phase) and coherence function were calculated from CSP input to SNA in the baroreflex neural arc and from SNA input to AP in the baroreflex peripheral arc. The signals of CSP, SNA and AP were resampled at 10 Hz and segmented into 10 sets of 50% overlapping bins of 2^{10} data point each. The segment length was 102.4 s, which yielded the lowest frequency bound of 0.01 (0.0097) Hz. We subtracted a linear trend and applied a Hanning window for each segment. We then performed fast Fourier transform to obtain frequency spectra of the variables. We ensemble averaged the input power [$Sxx(f)$], output power [$Syy(f)$], and cross power between them [$Syx(f)$] over the 10 segments. Thereafter, we calculated the transfer function [$H(f)$] from input to output signals as follows,

$$H(f) = \frac{Syx(f)}{Sxx(f)}$$

To quantify the linear dependence between input to output signals in the frequency domain, we calculated the magnitude-squared coherence function [$Coh(f)$] as follows:

$$Coh(f) = \frac{|Syx(f)|^2}{Sxx(f)Syy(f)}$$

The coherence value ranges from zero to unity. Unity coherence indicates a perfect linear dependence between input and output signals, whereas zero coherence indicates total independence of these two signals.

Statistic analysis. All data are presented as means ± SD. Effects of upright tilt on baroreflex parameters were evaluated by repeated-measures analysis of variance. When the main effect was found to be significant, post hoc multiple comparisons were done using the Scheff's F-test to compare baroreflex controls between the supine and upright postures [11]. Differences were considered significant when $P < 0.05$.

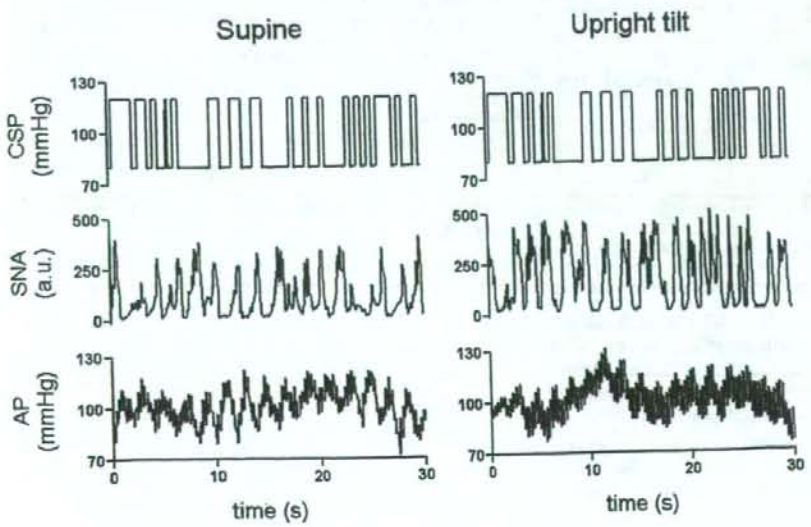

Fig. 2. Representative data of one rabbit in supine (left panels) and 60° upright tilt (right panels) positions, showing time series of carotid sinus pressure (CSP), sympathetic nerve activity (SNA) and systemic arterial pressure (AP) during CSP perturbation. CSP was changed according to a binary white noise signal with a switching interval of 500 ms. a.u., arbitrary unit.

RESULTS

Figure 2 shows the typical time series of CSP, SNA and AP derived in supine and 60° upright tilt positions in individual animal. CSP was perturbed according to a binary white noise sequence at 500-ms intervals. In both positions, SNA increased and decreased roughly in response to the decrease and increase in CSP, respectively. However, the SNA responses appeared higher in the upright tilt than in the supine position. Data from all animals (n = 8) showed that the upright tilt increased the averaged SNA (175 ± 21 a.u.) during CSP perturbation compared with the supine position (96 ± 13 a.u.). Averaged AP during CSP perturbation was similar in supine (96 ± 13 mmHg) and in upright positions (103 ± 15 mmHg).

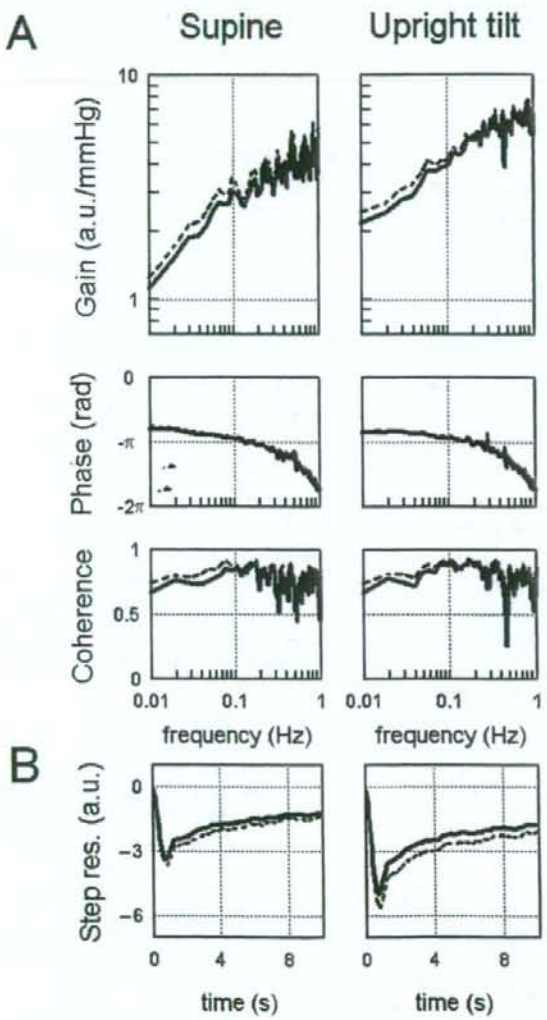

Fig. 3. A: The transfer function of the baroreflex neural arc from CSP to SNA averaged from all animals (n = 8) in supine (left panels) and 60° upright tilt (right panels) positions. The gain plots (top), phase plots (middle), and coherence function (bottom) are shown. Upright tilt increases the gain. **B**: Step responses (Step res.) derived from the transfer function corresponding to the transfer function shown in A. Upright tilt enhances the initial and steady-state responses. Solid line represents the mean values, and dashed line represents mean + SD in A and mean – SD in B. a.u., arbitrary unit.

The baroreflex neural arc

Figure 3A shows the transfer function of baroreflex neural arc from CSP to SNA averaged from all animals. In both supine and upright tilt positions, the transfer gain increased as the frequency of CSP perturbation increased for the frequency range of 0.01 to 1 Hz. This shows dynamic high-pass characteristics, indicating that more rapid change of CSP results in greater response of SNA. Note that upright tilt increased the transfer gain for the whole frequency range observed (Table 1). In addition, upright tilt decreased the slope of gain increase. In both positions, the phase approached slightly above $-\pi$ radians at the lowest frequency reflecting negative feedback characters, and lagged as the frequency of CSP perturbation increased. The coherence was over 0.7 for the frequency range of 0.01 to 0.2 Hz. Upright tilt did not affect the phase or coherence. Figure 3B shows the step response of SNA corresponding to the transfer function shown in Fig. 3A. In both positions, the SNA response consisted of an initial decrease followed by partial recovery and then a steady state. Of note, upright tilt enhanced the initial decrease by 50%, and also decreased the steady-state SNA.

Table 1. Transfer function of baroreflex neural arc (from CSP to SNA) in supine and upright tilt positions.

	Supine	Upright tilt
Gain (a.u./mmHg)		
0.01 Hz	1.11 ± 0.13	2.14 ± 0.41*
0.1 Hz	2.75 ± 0.43	4.63 ± 0.52*
0.3 Hz	3.69 ± 0.30	5.08 ± 0.42*
Phase (rad)		
0.01 Hz	–2.51 ± 0.15	–2.66 ± 0.09
0.1 Hz	–2.96 ± 0.08	–2.93 ± 0.06
0.3 Hz	–3.58 ± 0.14	–3.53 ± 0.12
Coherence		
0.01 Hz	0.67 ± 0.08	0.67 ± 0.07
0.1 Hz	0.84 ± 0.04	0.89 ± 0.02
0.3 Hz	0.77 ± 0.06	0.82 ± 0.03
Slope (dB/decade)		
0.01 Hz to 0.3 Hz	7.0 ± 0.4	5.1 ± 0.5*
Step response (a.u.)		
Initial response	–3.41 ± 0.21	–4.99 ± 0.62*
Steady-state level	–1.26 ± 0.18	–1.80 ± 0.32*

Values are mean ± SD (n =10). *P < 0.05; supine position vs. upright tilt.

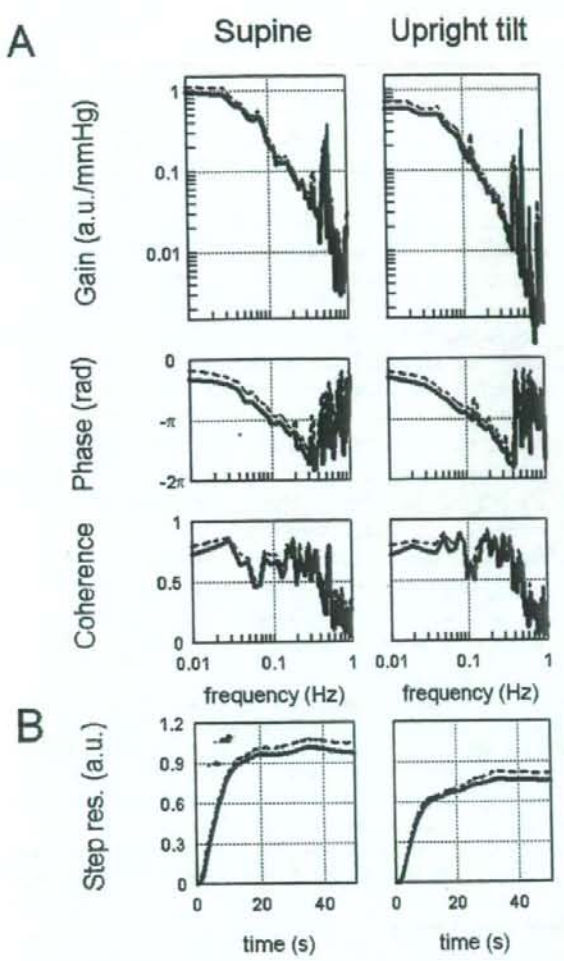

Fig. 4. A: The transfer function of the baroreflex peripheral arc from SNA to AP averaged from all animals (n = 8) in supine (left panels) and 60° upright tilt (right panels) positions. The gain plots (top), phase plots (middle), and coherence function (bottom) are shown. Upright tilt decreases the gain below the frequency of 0.1 Hz. **B**: Step responses (Step res.) derived from the transfer function corresponding to the transfer function shown in A. Upright tilt attenuates the response. Solid and dashed lines represent the mean and mean + SD values, respectively. a.u., arbitrary unit.

Table 2. Transfer function of baroreflex peripheral arc (from SNA to AP) in supine and upright tilt positions.

	Supine	Upright tilt
Gain (mmHg/au)		
0.01 Hz	0.97 ± 0.09	0.63 ± 0.06*
0.1 Hz	0.23 ± 0.03	0.15 ± 0.03*
0.3 Hz	0.04 ± 0.006	0.03 ± 0.003
Phase (rad)		
0.01 Hz	–0.79 ± 0.16	–0.69 ± 0.07
0.1 Hz	–2.83 ± 0.14	–2.58 ± 0.15
0.3 Hz	–4.74 ± 0.18	–4.63 ± 0.08
Coherence		
0.01 Hz	0.72 ± 0.07	0.71 ± 0.03
0.1 Hz	0.64 ± 0.08	0.62 ± 0.04
0.3 Hz	0.61 ± 0.08	0.68 ± 0.02
Step response (mmHg)		
Steady-state level	–0.97 ± 0.06	–0.75 ± 0.06*

Values are mean ± SD (n =10). *P < 0.05; supine position vs. upright tilt.

The baroreflex peripheral arc

Figure 4A shows the transfer function of the baroreflex peripheral arc from SNA to AP averaged from all animals. In both supine and upright tilt positions, the transfer gain decreased as the input frequency increased for the frequency range of 0.01 to 1 Hz, indicating low-pass characteristics. Upright tilt decreased the transfer gain between 0.01 and 0.1 Hz (Table 2). In both positions, the phase approached zero radian at the lowest frequency reflecting an increase in SNA with increased AP, and lagged as the input frequency increased. The coherence was over 0.5 for the frequency range of 0.01 to 1 Hz. Upright tilt did not affect the phase or coherence. Figure 4B shows the step response of AP corresponding to the transfer function shown in Fig. 4A. In both positions, the AP response increased gradually to reach a steady state. Upright tilt decreased the steady-state AP.

The total baroreflex arc

Figure 5A shows the transfer function of the total baroreflex arc from CSP to AP averaged from all animals. In both supine and upright tilt positions, the transfer gain decreased as the input frequency increased for the frequency range from 0.01 to 1 Hz, indicating low-pass characteristics. Upright tilt did not affect the transfer gain (Table 3). In both positions, the phase approached –π radians at the lowest frequency reflecting negative feedback attained by the total baroreflex loop, and lagged as the input frequency increased. The coherence was over 0.5 for the frequency range from 0.01 to 0.2 Hz. Upright tilt did not affect the phase or coherence. Figure 5B shows the step response of AP corresponding to the transfer function shown in Fig. 5A. In both positions, the AP response increased gradually to reach a steady state. Upright tilt did not affect the step response.

The right column of Table 3 shows a simulation of the total arc transfer function in the absence of resetting in the neural arc. The simulation was based on the neural arc transfer function in supine position and the peripheral arc transfer function in upright tilt position. Without the resetting, the upright tilt would decrease the transfer function gain and would attenuate the step response of AP at steady state, compared with the values in supine position and those in upright tilt position with resetting.

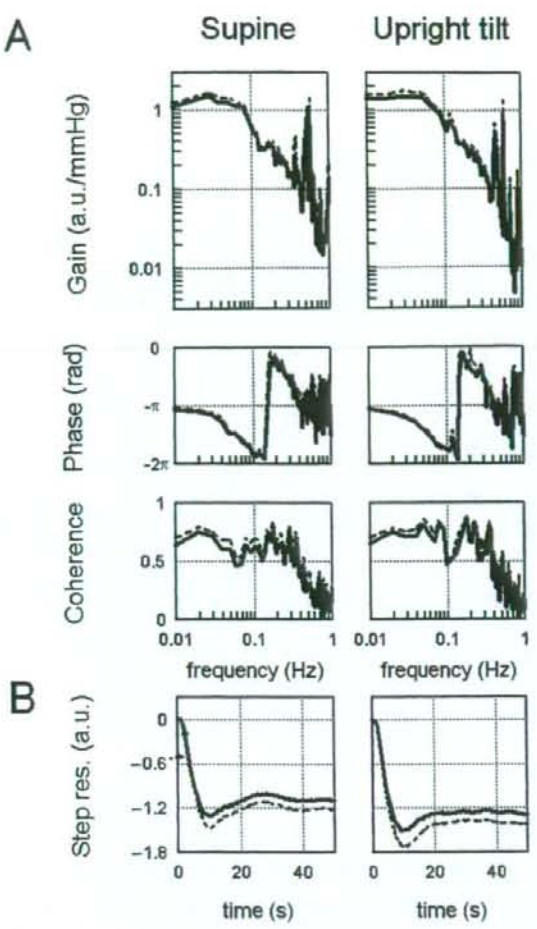

Fig. 5. A: The transfer function of the total baroreflex arc from CSP to AP averaged from all animals (n = 8) in supine (left panels) and 60° upright tilt (right panels) positions. The gain plots (top), phase plots (middle), and coherence function (bottom) are shown. **B**: Step responses (Step res.) derived from the transfer function corresponding to the transfer function shown in A. The transfer function and step response are similar in the supine and upright tilt positions. Solid and dashed lines represent the mean and mean + SD values in A and mean – SD values in B, respectively. a.u., arbitrary unit.

DISCUSSION

Arterial baroreflex is obviously a pivotal mechanism for maintaining AP under orthostatic stress against gravitational fluid shift and pressure disturbance [1, 2, 4], but the baroreflex function and its modulation in upright position are not fully understood. We previously reported that 60° upright tilt resets the steady-state characteristics of the baroreflex neural arc to a higher SNA [5]. However, the dynamic characteristics of the baroreflex system, which is a hallmark of fast-acting neural systems, in upright posture remain to be elucidated. Accordingly, in the present study, we identified the transfer function of the total baroreflex system and its two subsystems. The new major findings are that a 60° upright tilt increases the transfer gain of the baroreflex neural arc (CSP to SNA), decreases the transfer gain of the peripheral arc (SNA to AP), and as a result maintains the dynamic characteristics of the total baroreflex feedback system. These findings support our hypothesis that upright tilt resets dynamic transfer function of baroreflex neural arc to minify the pressure disturbance in total baroreflex control. These results were not affected by the order of postures, since returning the ani-

Table 3. Transfer function of total baroreflex arc (from CSP to AP) in supine, upright tilt and simulated upright tilt positions.

	Supine	Upright tilt	Simulated upright tilt without resetting of the neural arc
Gain (a.u./mmHg)			
0.01 Hz	1.10 ± 0.12	1.38 ± 0.18	0.71 ± 0.18*#
0.1 Hz	0.63 ± 0.09	0.69 ± 0.12	0.41 ± 0.13*#
0.3 Hz	0.15 ± 0.03	0.15 ± 0.03	0.11 ± 0.04*
Phase (rad)			
0.01 Hz	–3.33 ± 0.11	–3.29 ± 0.07	–3.21 ± 0.10
0.1 Hz	–5.76 ± 0.20	–5.55 ± 0.10	–5.51 ± 0.15
0.3 Hz	–1.98 ± 0.25	–1.87 ± 0.23	–1.91 ± 0.24
Coherence			
0.01 Hz	0.63 ± 0.06	0.65 ± 0.05	
0.1 Hz	0.60 ± 0.10	0.61 ± 0.06	
0.3 Hz	0.53 ± 0.07	0.55 ± 0.04	
Step response (mmHg)			
Steady-state level	–1.09 ± 0.11	–1.29 ± 0.12	–0.67 ± 0.11*#

Simulated transfer function in the absence of neural arc resetting is calculated from the neural arc transfer function in supine position and the peripheral arc transfer function in upright tilt position. Values are mean ± SD (n =10). *P < 0.05; supine vs. simulated upright tilt, #P < 0.05; upright tilt vs. simulated upright tilt.

mal posture from 60° upright tilt to horizontal supine position restored the transfer functions to the magnitudes observed in the initial supine position (data not shown).

Little is known about the arterial baroreflex feedback system under orthostatic stress. Although earlier studies investigated the gains of baroreflex control of SNA [12–14], vascular resistance [15] and R-R interval [16], these gains are parts of the total baroreflex system, and thus are insufficient to explain the dynamics of the total arc of the baroreflex feedback system. In addition, no study has examined the phase function of baroreflex in the subsystems and the total system. Moreover, while earlier studies addressed baroreflex in relation to AP regulation under orthostatic stress, most of them evaluated the baroreflex in supine, and not orthostatic posture [14]. In the present study, we identified the transfer functions of the two baroreflex subsystems (the neural and peripheral arcs) in upright posture independently using the baroreflex open-loop technique. Moreover, by connecting the subsystem transfer functions in series and closing them, we revealed the dynamic characteristics of the total baroreflex arc.

Our actual and simulation data indicated that resetting of the baroreflex neural arc in upright posture increases the transfer function gain of the total baroreflex arc. In our experiments, the 60° upright tilt reset and nearly doubled the transfer gain of the neural arc. Although the upright tilt decreased the transfer gain of the peripheral arc, resetting in the neural arc counteracted it and consequently preserved the dynamic transfer gain of the total baroreflex arc (1.4, Table 3). In a simulation of a situation where resetting in the neural arc is absent (Table 3), a 60° upright tilt would decrease the total arc transfer gain. These findings suggest that resetting of the neural arc (that is, baroreflex control of SNA) with dynamic characteristics plays an im-

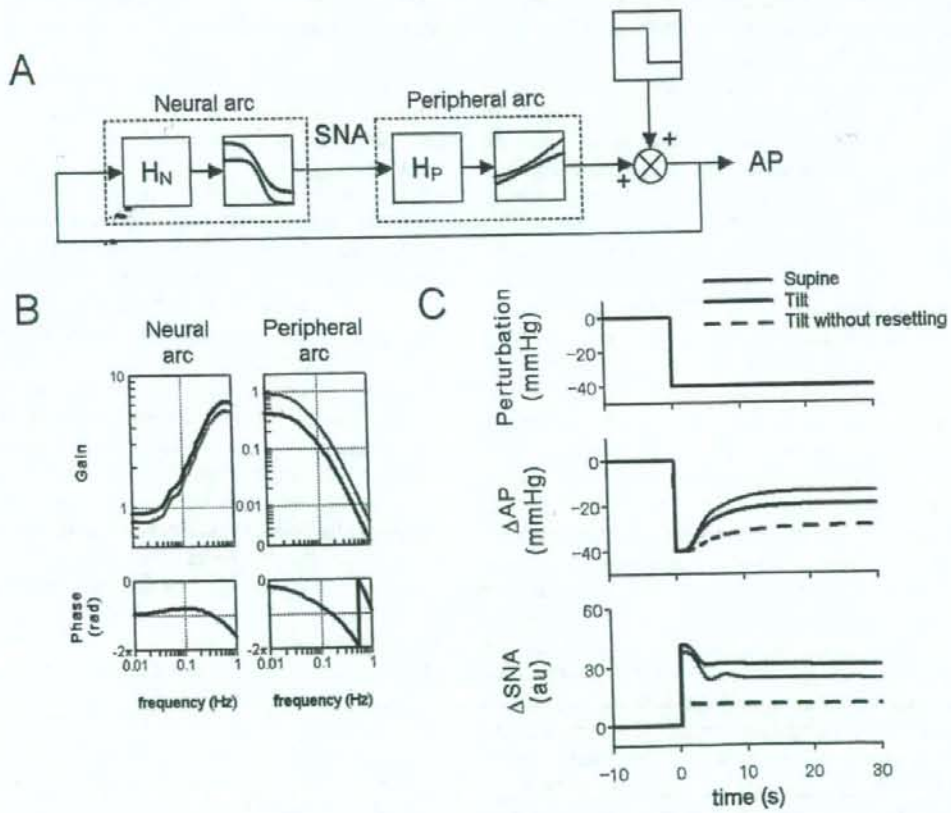

Fig. 6. A: Simulator of the baroreflex system during upright tilt. A stepwise perturbation was applied to the baroreflex negative feedback system (see APPENDIX for details). H_N, neural arc transfer function; H_P, peripheral arc transfer function. Nonlinear sigmoidal functions in the supine and upright tilt positions are shown by gray and black lines, respectively. **B:** Simulation results of integrated dynamic transfer function of linear-sigmoidal nonlinear cascade model in the neural (AP to SNA) and peripheral (SNA to AP) arcs in the supine (gray lines) and upright tilt (black lines) positions. **C:** Simulation results of a closed-loop AP and SNA responses to the stepwise pressure perturbation (–40 mmHg). The resetting during upright tilt (black line) would enhance SNA excitation as compared with the supine position (gray line) to minify a hypotension. Without the resetting in upright tilt, SNA responses would largely be attenuated to lead a hypotension.

portant role to maintain the dynamic transfer function of the total baroreflex system in upright posture.

A simulation of AP stability by baroreflex feedback control against pressure disturbance clearly suggests the importance of resetting of baroreflex neural arc in upright posture. Figure 6 shows the simulation of closed-loop baroreflex control of AP, when pressure disturbance was loaded to the peripheral cardiovascular compartment. According to an earlier study [17], we used the linear-sigmoidal nonlinear cascade model (Fig. 6A) to simulate the baroreflex dynamics. The result of simulation (Fig. 6B) was consistent with our in vivo findings that an upright tilt increased the dynamic transfer gain of the neural arc and decreased the dynamic gain of the peripheral arc. The simulation (Fig. 6C) shows that the baroreflex feedback system would minify the pressure disturbance (40 mmHg) by 50% or more in supine (14 mmHg) and upright tilt (19 mmHg) positions. However, without the resetting of the neural arc in upright tilt, the residual pressure disturbance (29 mmHg) would persist and the velocity of pressure response would become slower (Fig. 6C). These findings suggest that dynamic resetting of the neural arc increases the stability and quickness in response of orthostatic AP against pressure disturbance in closed-loop condition of the total baroreflex arc. In addition, the simulation indicates that the resetting would enhance increases in SNA in response to pressure disturbance in upright tilt compared to supine position (Fig. 6C). Without the resetting in upright tilt, the SNA response would be greatly attenuated (Fig. 6C). This suggests that resetting of the neural arc has a critical role in activating SNA appropriately to prevent hypotension by pressure disturbance during orthostatic stress.

Some explanations for the changes in baroreflex peripheral arc in upright tilt posture may be postulated. First, since the gravitational fluid shift toward the lower part of body (i.e., abdominal vascular bed, lower limbs) during upright posture decreases the preload and effective circulatory blood volume [1, 9], it may attenuate the dynamic transfer function from SNA to AP. Our actual data revealed that upright tilt decreased the transfer gain, but not the transfer phase, of the baroreflex peripheral arc (Fig. 4A). Therefore, upright tilt would blunt the magnitude of AP response to SNA without delaying the response, as shown in the calculated step response (Fig. 4B). Next, increases in humoral factors (i.e., catecholamine, angiotensin II) during upright posture could reduce the dependency of vascular resistance on neural control. However, intravenous infusion of angiotensin II did not affect the transfer function of baroreflex peripheral arc [18]. Moreover, intravenous infusion of catecholamine had no effects on the transfer function from sympathetic stimulation to heart rate [19]. These studies are consistent with the predominance of sympathetic neural control on cardiovascular pressor function [20].

Limitations

The present study has several limitations. First, we excluded the efferent effect of vagally mediated arterial and cardiopulmonary baroreflexes that may affect baroreflex control of SNA. Second, we used an anesthetic agent that may attenuate the baroreflex peripheral arc by reducing the cardiac pumping function, and may affect the neural arc gain. Third, since we sectioned the aortic depressor nerves to open the baroreflex feedback loop, the total baroreflex gain may be lower than the physiological level. Fourth, since we measured only renal SNA, our findings have limited applicability to other SNA. Although static [10, 21] and dynamic [21] regulation of the baroreflex neural arc is similar in renal, cardiac and muscle (vasoconstrictor) SNAs in supine posture, whether this holds true during orthostatic stress remains to be verified.

Lastly, we used rabbits that are quadrupeds. Since humans spend most of their time in nearly 90° upright postures whereas rabbits do not, our findings have limited applicability to humans. However, Japanese White rabbits spend most of their time in 10–40° head-up postures, and frequently stand up to nearly 70°. Since the denervation of both carotid and aortic arterial baroreflexes is known to cause severe postural hypotension at 60° upright tilt in quadrupeds [4], this suggests that even in quadrupeds, arterial baroreflex has a very important function in the maintenance of AP under orthostatic stress. Accordingly, despite the difference in species, our findings may reflect, at least, the qualitative aspects of orthostatic baroreflex physiology in humans. Indeed, recent human studies have suggested that orthostatic stress (lower body negative pressure) enhances the SNA response to AP change [22, 23] and increases baroreflex control of SNA (assessed by the relation between spontaneous changes in diastolic AP and SNA) [12] under baroreflex closed-loop condition.

In conclusion, the transfer function identified in baroreflex open-loop condition showed that 60° upright tilt increases the transfer gain of the baroreflex neural arc, decreases the transfer gain of the peripheral arc, and as a result maintains the dynamic characteristics of the total baroreflex feedback system. Simulation study suggests that resetting of the neural arc increases the transfer gain of the total baroreflex arc and also increases the stability of orthostatic AP against pressure disturbance. These findings suggest that upright tilt resets the dynamic transfer function of the baroreflex neural arc to maintain total baroreflex stability.

APPENDIX

To simulate the closed-loop AP response to stepwise pressure perturbation (Fig. 6), we used the linear-sigmoidal nonlinear cascade model [17].

We modeled the sigmoidal nonlinearity in the baroreflex neural arc by a four-parameter logistic function with

threshold according to our previous study [5] using the following equation:

$$y = \frac{P_1}{1+\exp[P_2(x-P_3)]} + P_4$$

where x and y are input (in mmHg) and output (in au) values. P_1 denotes the response range (in a.u.), P_2 is the coefficient of gain, P_3 is the midpoint of the input range (in mmHg), P_4 is the minimum output value of the symmetric sigmoid curve (in a.u.). We set $P_1 = 94$, $P_2 = 0.10$, $P_3 = 109$, $P_4 = 4$ in the supine position, and $P_1 = 112$, $P_2 = 0.09$, $P_3 = 109$, $P_4 = 29$ during upright tilt, according to our previous study [5].

The sigmoidal nonlinearity in the peripheral arc was modeled by a four-parameter logistic function using the following equation:

$$z = \frac{Q_1}{1+\exp[Q_2(y-Q_3)]} + Q_4$$

where y and z are input (in a.u.) and output (in mmHg) values. Q_1 denotes the response range (in mmHg), Q_2 is the coefficient of gain, Q_3 is the midpoint of the input range (in a.u.), and Q_4 is the minimum output value (in mmHg). We set $Q_1 = 115$, $Q_2 = -0.04$, $Q_3 = 63$, $Q_4 = 50$ in the supine position, and $Q_1 = 82$, $Q_2 = -0.05$, $Q_3 = 88$, $Q_4 = 50$ during upright tilt, according to our previous study [5].

In rabbits, the transfer function of the baroreflex neural arc (baroreceptor pressure to SNA) approximates derivative characteristics in the frequency range below 0.8 Hz, and high-cut characteristics of frequencies above 0.8 Hz [17]. Therefore, according to our previous study [17], we modeled the neural arc transfer function (H_N) using the following equation:

$$H_N(f) = -K_N \frac{1+\frac{f}{f_{c1}}j}{\left(1+\frac{f}{f_{c2}}\right)^2}\exp(-2\pi fjL)$$

where f and j represent the frequency (in Hz) and imaginary units, respectively; K_N is static gain (in a.u./mmHg); f_{c1} and f_{c2} ($fc_1 < f_{c2}$) are corner frequencies (in Hz) for derivative and high-cut characteristics, respectively; and L is a pure delay (in s) that would represent the sum of delays in the synaptic transmission through the baroreflex central pathways and the sympathetic ganglion. The dynamic gain increases in the frequency range of f_{c1} to f_{c2}, and decreases above f_{c2}. In simulations showed in Fig. 6, we matched K_N to the actual data in the supine and upright tilt positions in this study. We also set f_{c1}, f_{c2} and L at 0.05, 0.8 and 0.2, respectively, according to the present and previous studies [17].

In addition, the transfer function of the baroreflex peripheral arc (SNA to AP) approximates a second-order low-pass filter with the dead time as follows:

$$H_P(f) = K_P \frac{1}{1+2\zeta\frac{f}{f_N}j-\left(\frac{f}{f_N}\right)^2}\exp(-2\pi fjL)$$

where f_N and ζ are the neutral frequency (in Hz) and damping ratio, respectively; and L is a pure delay (in s). In simulations showed in Fig. 6, we matched K_P to the actual data in the supine and upright tilt positions in this study. We also set f_N, ζ and L at 0.07, 1.4 and 1.0, respectively, according to the present and previous studies [17].

The input amplitude of the stepwise pressure perturbation was –40 mmHg (Fig. 5, A and C, top panel). The closed-loop AP (Fig. 5C, middle panel) and SNA (Fig. 5C, bottom panel) responses were simulated up to 30 s.

This study was supported by the research project promoted by Ministry of Health, Labour and Welfare in Japan (#H18-nano-ippan-003), the Grants-in-Aid for Scientific Research promoted by Ministry of Education, Culture, Sports, Science and Technology in Japan (#18591992, #20390462) and the Industrial Technology Research Grant Program from New Energy and Industrial Technology Development Organization of Japan.

REFERENCES

1. Rowell LB. Human cardiovascular control. New York: Oxford Univ. Press, 1993.
2. Eckberg DL, Sleight P. Human baroreflexes in Health and Disease. New York: Oxford Univ. Press, 1992.
3. Persson P, Kirchheim H. Baroreceptor reflexes: integrative functions and clinical aspects. Berlin: Springer-Verlag, 1991.
4. Sato T, Kawada T, Sugimachi M, Sunagawa K. Bionic technology revitalizes native baroreflex function in rats with baroreflex failure. Circulation. 2002;106:730-4.
5. Kamiya A, Kawada T, Yamamoto K, Michikami D, Ariumi H, Uemura K, et al. Resetting of the arterial baroreflex increases orthostatic sympathetic activation and prevents postural hypotension in rabbits. J Physiol. 2005;566:237-46.
6. Sato T, Kawada T, Inagaki M, Shishido T, Takaki H, Sugimachi M, et al. New analytic framework for understanding sympathetic baroreflex control of arterial pressure. Am J Physiol. 1999;276:H2251-61.
7. Yamamoto K, Kawada T, Kamiya A, Takaki H, Miyamoto T, Sugimachi M, et al. Muscle mechanoreflex induces the pressor response by resetting the arterial baroreflex neural arc. Am J Physiol. 2004;286:H1382-8.
8. Ikeda Y, Kawada T, Sugimachi M, Kawaguchi O, Shishido T, Sato T, et al. Neural arc of baroreflex optimizes dynamic pressure regulation in achieving both stability and quickness. Am J Physiol. 1996;271:H882-90.
9. Sagawa K, Maughan L, Suga H, Sunagawa K. Cardiac contraction and the pressure-volume relationship. New York: Oxford Univ Press, 1988.
10. Kawada T, Shishido T, Inagaki M, Tatewaki T, Zheng C, Yanagiya Y, et al. Differential dynamic baroreflex regulation of cardiac and renal sympathetic nerve activities. Am J Physiol Heart Circ Physiol. 2001;280:H1581-90.
11. Glantz SA. Primer of Biostatistics (4th ed). New York: McGraw-Hill, 1997.
12. Ichinose M, Saito M, Fujii N, Kondo N, Nishiyasu T. Modulation of the control of muscle sympathetic nerve activity during severe orthostatic stress. J Physiol. 2006;576:947-58.
13. Fu Q, Shook RP, Okazaki K, Hastings JL, Shibata S, Conner CL, et al. Vasomotor sympathetic neural control is maintained during sustained upright posture in humans. J Physiol (Lond). 2006;577:679-87.
14. Mosqueda-Garcia R, Furlan R, Fernandez-Violante R, Desai T, Snell M, Jarai Z, et al. Sympathetic and baroreceptor reflex function in neurally mediated syncope evoked by tilt. J Clin Invest. 1997;99:2736-44.
15. Cooper VL, Hainsworth R. Carotid baroreceptor reflexes in humans during orthostatic stress. Exp Physiol. 2001;86:677-81.
16. Cooke WH, Hoag JB, Crossman AA, Kuusela TA, Tahvanainen KU, Eckberg DL.

Human responses to upright tilt: a window on central autonomic integration. J Physiol. 1999;517:617-28.
17. Kawada T, Yanagiya Y, Uemura K, Miyamoto T, Zheng C, Li M, et al. Input-size dependence of the baroreflex neural arc transfer characteristics. Am J Physiol Heart Circ Physiol. 2003;284:H404-15.
18. Kashihara K, Takahashi Y, Chatani K, Kawada T, Zheng C, Li M, et al. Intravenous angiotensin II does not affect dynamic baroreflex characteristics of the neural or peripheral arc. Jpn J Physiol. 2003;53:135-43.
19. Kawada T, Miyamoto T, Miyoshi Y, Yamaguchi S, Tanabe Y, Kamiya A, et al. Sympathetic neural regulation of heart rate is robust against high plasma catecholamines. J Physiol Sci. 2006;56:235-45.
20. Minson J, Chalmers J, Kapoor V, Cain M, Caon A. Relative importance of sympathetic nerves and of circulating adrenaline and vasopressin in mediating hypertension after lesions of the caudal ventrolateral medulla in the rat. J Hypertens. 1986;4:273-81.
21. Kamiya A, Kawada T, Yamamoto K, Michikami D, Ariumi H, Miyamoto T, et al. Muscle sympathetic nerve activity averaged over 1 minute parallels renal and cardiac sympathetic nerve activity in response to a forced baroreceptor pressure change. Circulation. 2005;112:384-6.
22. Ichinose M, Saito M, Ogawa T, Hayashi K, Kondo N, Nishiyasu T. Modulation of control of muscle sympathetic nerve activity during orthostatic stress in humans. Am J Physiol Heart Circ Physiol. 2004;287:H2147-53.
23. Ichinose M, Saito M, Kitano A, Hayashi K, Kondo N, Nishiyasu T. Modulation of arterial baroreflex dynamic response during mild orthostatic stress in humans. J Physiol. 2004;557:321-30.

Life Sciences 83 (2008) 490–495

Contents lists available at ScienceDirect

Life Sciences

journal homepage: www.elsevier.com/locate/lifescie

Vagal stimulation suppresses ischemia-induced myocardial interstitial myoglobin release

Toru Kawada [a,*], Toji Yamazaki [b], Tsuyoshi Akiyama [b], Hirotoshi Kitagawa [c], Shuji Shimizu [a], Masaki Mizuno [a], Meihua Li [a], Masaru Sugimachi [a]

[a] Department of Cardiovascular Dynamics, Advanced Medical Engineering Center, National Cardiovascular Center Research Institute, Osaka 565-8565, Japan
[b] Department of Cardiac Physiology, National Cardiovascular Center Research Institute, Osaka 565-8565, Japan
[c] Department of Anesthesiology, Shiga University of Medical Science, Shiga 520-2192, Japan

ARTICLE INFO

Article history:
Received 19 May 2008
Accepted 23 July 2008

Keywords:
Coronary artery occlusion
Cardiac microdialysis
Cats

ABSTRACT

Aims: To evaluate vagal stimulation-mediated myocardial protection against ischemia and reperfusion in in vivo ischemic myocardium.
Main methods: We measured myocardial interstitial myoglobin levels in the ischemic region using a cardiac microdialysis technique in anesthetized and vagotomized cats. We occluded the left anterior descending coronary artery (LAD) for 60 min and reperfused it for 60 min (VX group, $n=6$). The effects of bilateral vagal stimulation (10 V, 5 Hz, 1-ms pulse duration), initiated immediately after LAD occlusion, were examined (VS group, $n=6$). To examine the involvement of phosphatidylinositol 3-kinase (PI3K), vagal stimulation was performed after pretreatment with a PI3K inhibitor wortmannin (0.6 mg/kg, i.v.) (VS-W group, $n=6$). To examine the contribution of bradycardia, vagal stimulation was performed with fixed-rate ventricular pacing (VS-P group, $n=6$).
Key findings: The average myoglobin level during the ischemic period was 1170±141 in VX (in ng/ml, mean±SE), which was significantly attenuated in VS (466±87, $P<0.05$) and VS-W (613±124, $P<0.05$) but not in VS-P (953±203). Reperfusion increased the myoglobin level to 2500±544 in VX, whereas it was suppressed in VS (824±213, $P<0.05$) and VS-W (948±315, $P<0.05$) but not in VS-P (1710±253).
Significance: Vagal stimulation, initiated immediately after LAD occlusion, attenuated the myocardial injury. Moreover, bradycardia, independent of PI3K pathway, plays a significant role in vagally induced cardioprotection during acute myocardial ischemia.

Introduction

An increase in parasympathetic tone can provide cardioprotection against acute myocardial ischemia and infarction via the direct effects of acetylcholine (ACh) on the ischemic myocardium and the indirect effects mediated by altered hemodynamics. For the direct effects, administration of ACh prior to a coronary artery occlusion reduces the infarct size in isolated, perfused rabbit heart (Qin et al., 2003). Phosphatidylinositol 3-kinase (PI3K) is thought to be an upstream enzyme in the signal transduction pathway for the ACh-induced, ischemic preconditioning mimetic effect (Qin et al., 2003; Oldenburg et al., 2003). For the indirect effects, vagal stimulation reduces myocardial oxygen consumption due to bradycardia (Sammel et al., 1983) and also decreases ventricular contractility via antagonism of the sympathetic effect (Nakayama et al., 2001). Vagal stimulation can also dilate the coronary artery (Feigl, 1969; Reid et al., 1985; Feliciano and Henning, 1998; Henning and Sawmiller, 2001), which may increase collateral flow into the ischemic region.

In a previous study, we demonstrated that efferent vagal stimulation nearly halved the increase in myocardial interstitial norepinephrine levels in the ischemic region of the feline ventricle (Kawada et al., 2006). Whether vagal stimulation can reduce myocardial damage in the ischemic region, however, has yet to be directly examined. To test the hypothesis that vagal stimulation reduces myocardial injury in the ischemic region, we measured myocardial interstitial myoglobin levels during acute myocardial ischemia and reperfusion with or without efferent vagal stimulation in anesthetized cats. We examined possible involvement of the PI3K signaling pathway using vagal stimulation and pretreatment with a PI3K inhibitor wortmannin. We also examined the contribution of bradycardia using vagal stimulation and fixed-rate ventricular pacing.

Materials and methods

Surgical preparation

Animal care was provided in strict accordance with the *Guiding Principles for the Care and Use of Animals in the Field of Physiological Sciences* approved by the Physiological Society of Japan. Adult cats

* Corresponding author. Department of Cardiovascular Dynamics, National Cardiovascular Center Research Institute, 5-7-1 Fujishirodai, Suita, Osaka 565-8565, Japan. Tel.: +81 6 6833 5012x2427; fax: +81 6 6835 5403.
E-mail address: torukawa@res.ncvc.go.jp (T. Kawada).

0024-3205/$ – see front matter © 2008 Elsevier Inc. All rights reserved.
doi:10.1016/j.lfs.2008.07.013